


Cite this: *Chem. Sci.*, 2022, 13, 159

All publication charges for this article have been paid for by the Royal Society of Chemistry

# High-efficiency hyperfluorescent white light-emitting diodes based on high-concentration-doped TADF sensitizer matrices *via* spatial and energy gap effects†

Chunbo Duan,‡ Ying Xin,‡ Zicheng Wang, Jing Zhang, Chunmiao Han and Hui Xu \*

Despite the success of monochromatic hyperfluorescent (HF) organic light-emitting diodes (OLEDs), high-efficiency HF white OLEDs (WOLEDs) are still a big challenge. Herein, we demonstrate HF WOLEDs with state-of-the-art efficiencies, featuring a quasi-bilayer emissive layer (EML) composed of an ultrathin (0.1 nm) blue fluorescence (FL) emitter (TBPe) layer and a layer of thermally activated delayed fluorescence (TADF) sensitizer matrix heavily doped with a yellow FL emitter (TBRb, 3%). Based on an asymmetric high-energy-gap TADF sensitizer host (PhCzSPOTz), such an “ultrathin blue emitting layer (UTBL)” strategy endowed the HF WOLEDs with a record power efficiency of  $\sim 80 \text{ lm W}^{-1}$ , approaching the level of fluorescent tubes. Transient photoluminescence (PL) and electroluminescence (EL) kinetics demonstrate that the spatial separation of TBPe from the TADF sensitizer and TBRb, and the large energy gap between the latter two effectively suppress triplet leakage, in addition to suppressing triplet diffusion in the PhCzSPOTz matrix with anisotropic intermolecular interactions. These results provide a new insight into the exciton allocation process in HF white light-emitting systems.

Received 19th October 2021  
Accepted 24th November 2021

DOI: 10.1039/d1sc05753g

rsc.li/chemical-science

## 1. Introduction

White organic light-emitting diodes (WOLEDs) hold great promise for developing low-cost, energy-saving, environmentally friendly and eye-protecting solid-state lighting sources.<sup>1–5</sup> Compared to their fluorescence (FL) and phosphorescence (PH) counterparts, recently emerging thermally activated delayed fluorescence (TADF) materials and diodes have the advantages of power conservation, cost reduction and resource sustainability, since most of the TADF materials are pure-organic systems featuring near-zero singlet-triplet splitting ( $\Delta E_{\text{ST}}$ ) based efficient reverse intersystem crossing (RISC) for theoretically 100% exciton harvesting.<sup>6–11</sup> In this sense, TADF systems are almost “ideal” for WOLED applications.<sup>12</sup> Therefore, both all-TADF<sup>13–22</sup> and TADF-PH hybrid WOLEDs<sup>23–27</sup> were developed, which already realized the state-of-the-art performance comparable to PH WOLEDs, *e.g.* external quantum efficiencies

(EQE,  $\eta_{\text{EQE}}$ ) beyond 20%.<sup>28–32</sup> These systems provide multiple channels for triplet exciton harvesting. However, triplet excited state-involved processes are very complicated, including not only RISC and intersystem crossing (ISC) transitions, but also Dexter energy transfer (DXET) and intermolecular charge transfer (CT),<sup>33–35</sup> leading to a challenge of rational and balanced triplet exciton allocation for combining high electroluminescence (EL) efficiencies and white color purities.<sup>36–39</sup>

Actually, for a complementary white-emitting system composed of blue and yellow TADF or “TADF + PH” emitters, high-efficiency blue TADF dopants are commonly indispensable, but still inferior in availability and stability.<sup>40,41</sup> Although recently demonstrated synergistic effects between blue and yellow TADF dopants released more space for material selection and combination,<sup>42</sup> the excitation allocation is nonetheless limited by the contradiction between  $\eta_{\text{EUE}}$  and emission color purity, due to the different exciton utilization abilities of the emitters. A feasible strategy to solve this issue is simplifying the exciton allocation process, for which the TADF sensitized FL technology, known as hyperfluorescence (HF), provides a promising alternative.<sup>43,44</sup> For a complementary white HF system, a TADF sensitizer was used to complete triplet-to-singlet conversion and support subsequent Förster resonance energy transfer (FRET) to blue and yellow FL dopants.<sup>45,46</sup> In this “ideal” case, the exciton allocation only depends on singlet-exciton-involved FRET between TADF hosts and FL dopants, however, which should be based on the prevention of DEXT from the first

Key Laboratory of Functional Inorganic Material Chemistry, Ministry of Education & School of Chemistry and Material Science, Heilongjiang University, 74 Xuefu Road, Harbin 150080, P. R. China. E-mail: hxu@hlju.edu.cn

† Electronic supplementary information (ESI) available: Experimental details, single crystal data, thermal and solvatochromic properties, device performances, Gaussian simulation and photophysical results, electrochemical analysis and EL kinetics. CCDC 2099961, 1838785 and 1838786. For ESI and crystallographic data in CIF or other electronic format see DOI: 10.1039/d1sc05753g

‡ These authors contributed equally.

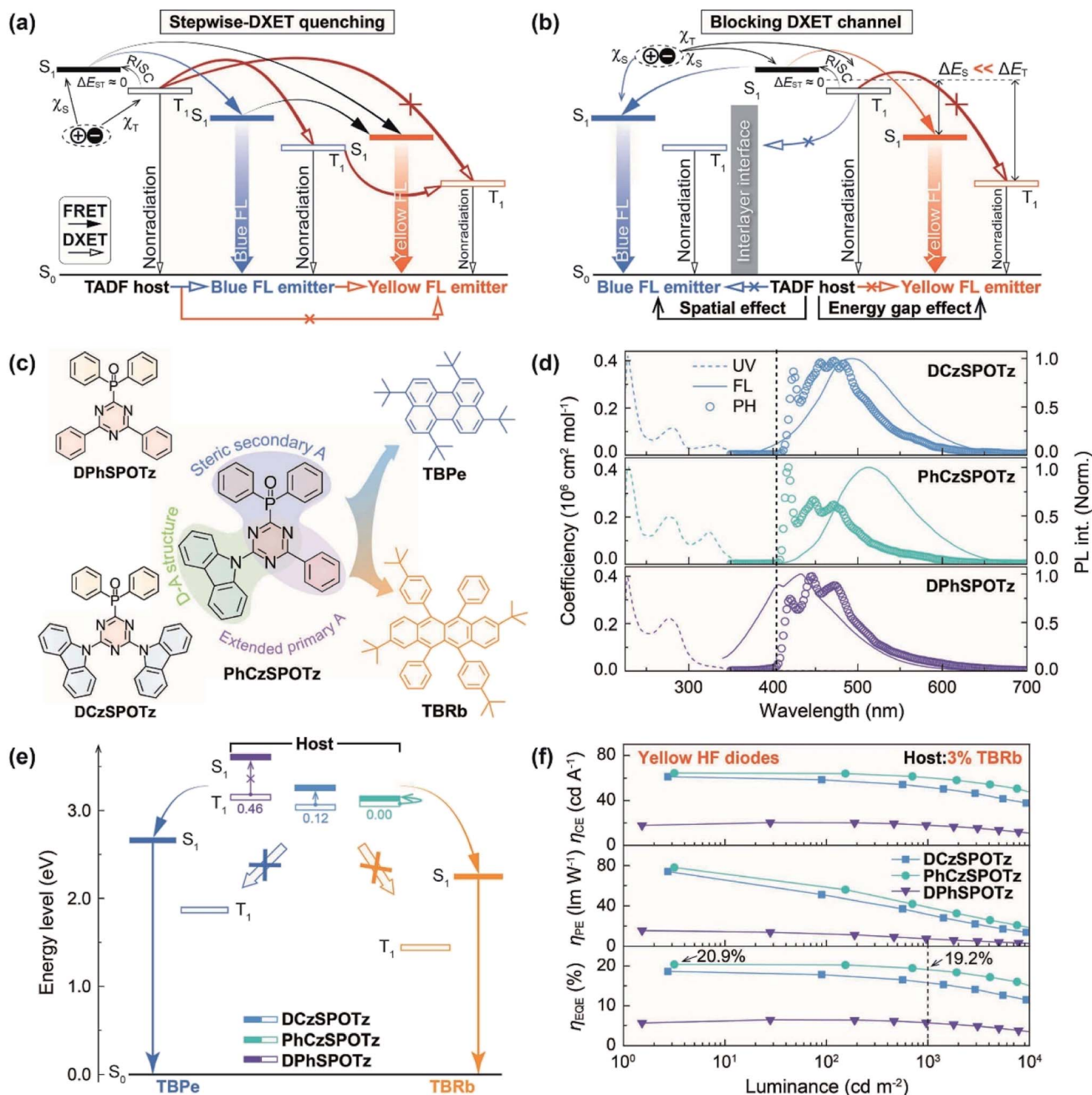


**Fig. 1** Design strategy of combining spatial and energy gap effects for TADF sensitized fluorescence systems. (a) Exciton allocation in a traditional TADF host sensitized complementary hyperfluorescent (HF) white system, featuring stepwise energy transfer, in which both singlet Förster resonance energy transfer (FRET) and triplet Dexter energy transfer (DXET) are involved and facilitated by the synergistic effect between blue and yellow FL emitters. To avert DXET-based triplet quenching by FL dopants, extremely low dopant concentrations (<1%) are required, but inducing the contradiction between exciton harvesting efficiencies and white color quality; (b) exciton allocation in a modified quasi-bilayer system consisting of an ultrathin host-free blue FL layer and a TADF-sensitized yellow FL layer, in which DXET from the TADF host to blue and yellow FL emitters is respectively restrained by spatial separation and a large triplet gap. This form simultaneously eliminates the synergistic effect of FL emitters in triplet wastage; (c) molecular design of two ternary TADF-type hosts DCzSPOTz and PhCzSPOTz composed of a carbazole (Cz) donor, triazine (Tz) primary acceptor and diphenylphosphine oxide (DPPO) secondary acceptor, respectively, and a n-type Tz-DPPO hybrid host DPhSPOTz for comparison. 1,4,7,10-Tetra(*tert*-butyl)perylene (TBPe) and 2,8-di-*tert*-butyl-5,11-bis(4-*tert*-butylphenyl)-6,12-diphenyltetracene (TBRb) were used as blue and yellow FL emitters; (d) electronic absorption and fluorescence at room temperature and time-resolved phosphorescence spectra (at 77 K after a 300  $\mu\text{s}$  delay) in  $\text{CH}_2\text{Cl}_2$  ( $10^{-5} \text{ mol L}^{-1}$ ) of the hosts; (e) excited-state energy level diagram of the hosts and FL emitters; (f) efficiency-luminance relationships of yellow FL diodes, respectively, using DCzSPOTz (square symbols), PhCzSPOTz (round symbols), and DPhSPOTz (lower triangle symbols) as hosts, whose emissive layers adopted high doping structures of host:3% TBRb.

triplet excited state ( $T_1$ ) of TADF sensitizers to the unusable  $T_1$  state of FL dopants (Fig. 1a). Therefore, nearly all HF diodes adopted additional host matrices to dilute TADF sensitizers and extremely low doping concentrations of FL emitters ( $\leq 1\%$ ) to reduce short-distance featured triplet DEXT,<sup>47</sup> but simultaneously limit the space for emission color tuning of white HF systems, which is actually another embodiment of the exciton allocation issue.<sup>48</sup> As a result, there have been very few all-HF WOLEDs reported to date.<sup>49–52</sup>

It is noted that since  $\Delta E_{ST}$  values (nearly zero) of TADF sensitizers are far smaller than those of FL dopants (commonly  $>0.5$  eV), the triplet energy gaps (EG) between TADF and FL molecules are correspondingly larger than their singlet EGs. It is known that energy transfer between two energy levels with a large energy gap is not efficient due to nonradiative deactivation during the energy transfer process. Therefore, by virtue of the EG effect, triplet DXET to FL dopants can be reduced by properly increasing the excited energy levels of TADF sensitizers, at the same time of preserving effective enough singlet FRET. Nonetheless, in a dually doped white single emissive layer (sEML), both the  $T_1$  energy levels of two FL dopants can induce triplet quenching. More importantly, the  $T_1$  energy levels of blue FL emitters between those of TADF sensitizers and yellow FL emitters reduce the triplet EGs, therefore facilitating the triplet DXET to yellow FL dopants, leading to the synergistic and amplification effects on triplet quenching (Fig. 1a). To avoid this issue, a common approach is to employ a white dual-emissive-layer (dEML) stack,<sup>53</sup> in which the blue and yellow FL dopants are respectively dispersed and spatially separated in two layers of the same or different host matrices, therefore suppressing blue-to-yellow DXET. Nevertheless, the triplet quenching by blue FL dopants still remains. Furthermore, rational exciton allocation is a challenge to each layer of the bilayer structure for efficient white emission, leading to more restricted and accurate requirements of the optoelectronic properties of host matrices.<sup>54</sup>

Herein, we put forward a structural design of HF WOLEDs based on a quasi-bilayer emissive layer (EML) consisting of an ultrathin host-free blue FL layer ( $<1$  nm) and a yellow host-dopant layer, namely the “UTBL” strategy (Fig. 1b). As a proof of concept, two molecules named DCzSPOTz and PhCzSPOTz are constructed as TADF sensitizer matrices (Fig. 1c), composed of carbazole (Cz) as a donor, and triazine (Tz) and diphenylphosphine oxide (DPPO) as primary and secondary acceptors, respectively. It is inspiring that based on the “UTBL” strategy, PhCzSPOTz endowed its HF WOLEDs with the state-of-the-art  $\eta_{EQE}$  up to 20.9%, which are largely improved by 3.5 and 5.2 fold, in comparison to the corresponding sEML and dEML-structured WOLEDs, respectively. More significantly, a record-high power efficiency (PE,  $\eta_{PE}$ ) of 78.3 lm W<sup>-1</sup> was achieved by these HF WOLEDs, demonstrating their great competence and potential for low-cost large-scale lighting applications.

## 2. Results and discussion

### 2.1. Design and structures

According to the “UTBL” strategy, in addition to EG effect-suppressed triplet quenching in the yellow FL layer, the host-

free feature of the UTBL amplifies the spatial effect, which averts direct interactions to TADF sensitizers, therefore further reducing the triplet leakage to blue FL emitters. In an ideal situation, the UTBL mainly utilizes electrogenerated singlet excitons, accompanied by FRET from TADF sensitizers in the adjacent doped EML, while, triplet excitons are thoroughly confined on TADF sensitizers and further upconverted to singlet excitons mostly transferring to yellow FL dopants (Fig. 1b). Obviously, the effectiveness of the “UTBL” strategy significantly depends on accurate exciton allocation to blue and yellow FL emitters, especially through exciton diffusion in the yellow doped EML and to the UTBL interface.

With this consideration, excited-state characteristics and intermolecular interactions of TADF sensitizer hosts should be carefully engineered. Accordingly, we designed and prepared symmetric DCzSPOTz and asymmetric PhCzSPOTz with the same donors and acceptors, as well as monopolar DPhSPOTz for comparison (Fig. 1c). The single crystal packing diagram of DCzSPOTz reveals relatively stronger intermolecular  $\pi$ - $\pi$  stacking interactions between adjacent Cz groups (Fig. S1†). On the contrary, no interactions are observed in the DPhSPOTz crystal, due to the predominant steric effect of DPPO. The asymmetric configuration of PhCzSPOTz induces staggering between adjacent Cz groups, therefore excluding  $\pi$ - $\pi$  stacking, but preserves weak interactions between DPPO groups. As a consequence, the intermolecular interaction intensity of PhCzSPOTz is between those of DCzSPOTz and DPhSPOTz, in accord with their melting points (Fig. S2†).

Compared to DCzSPOTz, the acceptor conjugation of PhCzSPOTz is extended by bonding Tz with a phenyl, which can further enhance the intramolecular charge transfer (ICT) interaction. As a result, the photoluminescence (PL) of PhCzSPOTz reveals bathochromic shifts over 10 nm and more marked solvatochromic effect (Fig. 1d and S3†). It is believed that ICT enhancement can facilitate frontier molecular orbital (FMO) separation for  $\Delta E_{ST}$  reduction and RISC improvement. According to the absorption edges and  $0 \rightarrow 0$  vibrational peaks of PH spectra in a dilute solution, PhCzSPOTz shows the almost equivalent single-molecular first singlet ( $S_1$ ) and  $T_1$  energy levels of 3.04 eV, corresponding to a negligible  $\Delta E_{ST}$  (Table S1†). In contrast, DCzSPOTz has an equal  $T_1$  level of 3.02 eV but a higher  $S_1$  level of 3.14 eV, resulting in a markedly larger  $\Delta E_{ST}$  value of 0.12 eV. The monopolar characteristics of DPhSPOTz give rise to the highest  $T_1$  value and the biggest  $\Delta E_{ST}$  among these phosphine oxide (PO) molecules. Nonetheless, all these PO hosts can support positive energy transfer to blue and yellow FL emitters, e.g. 1,4,7,10-tetra(*tert*-butyl)perylene (TBPe) ( $S_1 = 2.68$  eV) and 2,8-di-*tert*-butyl-5,11-bis(4-*tert*-butylphenyl)-6,12-diphenyltracene (TBRb) ( $S_1 = 2.26$  eV). It is noted that triplet gaps between all these PO hosts and TBRb are large enough ( $>0.8$  eV) to suppress triplet DXET (Fig. 1e).

### 2.2. OLED performance

To manifest the EG effect on suppressing triplet leakage, we fabricated yellow HF diodes with a four-layer structure of ITO|MoO<sub>3</sub> (6 nm)|1,1-bis(4-bis(4-methylphenyl)aminophenyl)





cyclohexane (TAPC, 40 nm)|4,4',4''-tris(carbazol-9-yl)-triphenylamine (TCTA, 10 nm)|PO host:TBRb (x%, 15 nm)|4,6-bis(diphenylphosphoryl)dibenzothiophene (DBTDPO, 40 nm)|LiF (1 nm)|Al (Fig. 1f and S4–S6†). As expected, in contrast to only 6.4%  $\eta_{\text{EQE}}$  of DPhSPOTz based analogs, at a relatively high TBRb concentration of  $x\% = 3\%$ , PhCzSPOTz endowed its device with the state-of-the-art performance (Fig. S5 and Table S2†), including 20.9% of  $\eta_{\text{EQE}}$  and  $78.3 \text{ lm W}^{-1}$  of  $\eta_{\text{PE}}$  for the maxima, and 19.2% of  $\eta_{\text{EQE}}$  at  $1000 \text{ cd m}^{-2}$ , respectively. In comparison,

the efficiencies of DCzSPOTz based diodes were lower, but still reached 18.7% and  $74.0 \text{ lm W}^{-1}$  for the maxima. Obviously, even at  $x > 1$ , triplet leakage to TBRb was still mostly prevented by the EG effect of DCzSPOTz and PhCzSPOTz matrices.

However, at doping concentrations of 0.5–5.0%, DCzSPOTz and PhCzSPOTz and TBPe based blue HF devices revealed serious triplet quenching, whose efficiencies were even markedly lower than those of DPhSPOTz based analogs (Fig. S7–S9 and Table S2†). We then fabricated sEML-type WOLEDs with

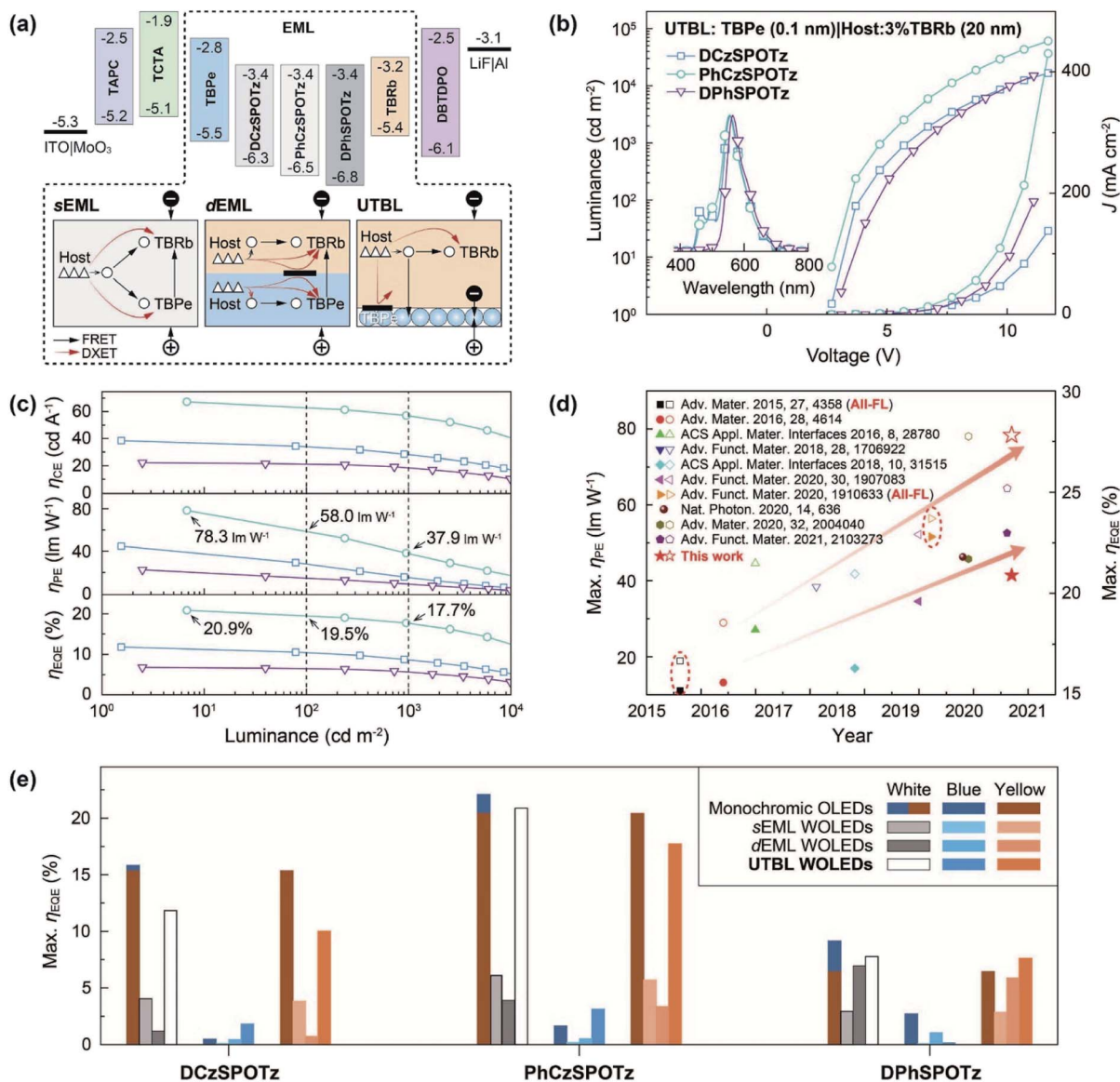


Fig. 2 EL performance of HF WOLEDs with single, dual and quasi-dual emissive layers. (a) Structural design and proposed energy transfer processes of HF WOLEDs, respectively, employing single (sEML) and dual (dEML) emissive layers (EML) as host:x% TBPe:y% TBRb, host:x% TBPe|host:y% TBRb, and quasi-dual EML of TBPe ( $\leq 0.5 \text{ nm}$ )|host:y% TBRb with an ultrathin blue layer (UTBL), in which round and triangle symbols refer to singlet and triplet excitons; (b) current density ( $J$ )–voltage–luminance curves and EL spectra (inset) of UTBL WOLEDs with  $y = 3$  at 5 V. EL performances of UTBL WOLEDs with other  $y$  values are presented in the ESI†; (c) efficiencies vs. luminance relationships of UTBL WOLEDs with  $y = 3$ ; (d) comparison between external quantum efficiencies (EQE,  $\eta_{\text{EQE}}$ , solid symbols) and power efficiencies (PE,  $\eta_{\text{PE}}$ , hollow symbols) of the representative TADF-FL hybrid and HF (marked with red dashed circles) WOLEDs reported so far, in which the values achieved by PhCzSPOTz hosted UTBL WOLEDs are highlighted with red star symbols; (e) comparison between the integral maximum  $\eta_{\text{EQE}}$  values and corresponding blue and yellow proportions of sEML, dEML and UTBL WOLEDs based on different hosts. The integral maximum  $\eta_{\text{EQE}}$  values of monochromatic blue and yellow diodes were included for comparison.

the same stacks, except for the EMLs of host:1.0% TBPe:y% TBRb (Fig. 2a, S10–S12 and Table S2†). Although the maximum luminance largely increased, the maximum efficiencies of DPhSPOTz based sEML WOLEDs were nearly the same as those of its blue diodes, due to FRET-predominant exciton allocation. In contrast, codoping TBRb markedly increased the maximum efficiencies of DCzSPOTz and PhCzSPOTz hosted sEML WOLEDs by 2.5–8 fold, since TBRb is superior to TBPe in exciton utilization. On the contrary, based on dual EMLs of host:1.0% TBPe|host:y% TBRb, DPhSPOTz supported its dEML WOLEDs with efficiencies similar to its yellow devices, which is opposite to the situations of DCzSPOTz and PhCzSPOTz hosted dEML WOLEDs with efficiencies even less than those of their sEML WOLEDs (Fig. S13–S15†). It is shown that despite spatial separation of two EMLs, exciton utilization by dEML structures reversely depends on the balance of exciton quenching in each layer. Consequently, more serious quenching in TBPe doped EMLs of DCzSPOTz and PhCzSPOTz hosted dEML WOLEDs directly drags down the total efficiencies.

We further used a non-doped ultrathin TBPe layer instead of a doped blue EML in dEML WOLEDs (Fig. S16–S18†). It is noted that the performance of these UTBL-type WOLEDs with EML structures of  $x$  nm TBPe|host:3% TBRb was highly sensitive to the TBPe thickness. Increasing  $x$  induced device efficiencies first increased at  $x \leq 0.1$ , and then decreased. At the turning point of  $x = 0.1$ , DCzSPOTz and PhCzSPOTz hosted UTBL WOLEDs displayed the similar dual-peak EL spectra, corresponding to warm-white emissions with CIE coordinates of about (0.40, 0.50) and a correlated color temperature (CCT) of  $\sim 4000$  K, which were close to those of standard warm-white illuminant A (Fig. 2b and Table S2†).

More importantly, PhCzSPOTz hosted UTBL WOLEDs realized the state-of-the-art efficiencies, *e.g.*  $\eta_{\text{EQE}}$  values of 20.9% for the maximum, and 19.4% and 17.7% at 100 and 1000  $\text{cd m}^{-2}$ , respectively (Fig. 2c and Table S2†). Owing to the reduced driving voltages, a record-high  $\eta_{\text{PE}}$  was realized as 78.3  $\text{lm W}^{-1}$  for the maximum, and remained as 58.4  $\text{lm W}^{-1}$  at 100  $\text{cd m}^{-2}$ , which were comparable to those of commercial fluorescent lamps, and therefore made PhCzSPOTz-hosted UTBL WOLEDs competent for low-power lighting applications. Furthermore,  $\eta_{\text{EQE}}$  roll-offs at 100 and 1000  $\text{cd m}^{-2}$  were as low as 7% and 15%, respectively. Consequently, PhCzSPOTz supported its UTBL WOLEDs with the best comprehensive performance reported so far among HF WOLEDs,<sup>51</sup> which was also comparable to those of the PH and TADF counterparts (Fig. 2d). In comparison,  $\eta_{\text{EQE}}$  values of DCzSPOTz-hosted UTBL WOLEDs were nearly halved to 11.8% for the maximum, and 10.4% and 8.8% at 100 and 1000  $\text{cd m}^{-2}$ , respectively, which were about the average  $\eta_{\text{EQE}}$  values of DCzSPOTz-based blue and yellow diodes. The contribution of TBPe to EL emissions of DPhSPOTz-based UTBL diodes was very limited, leading to the device performances consistent to its yellow diodes due to the similar exciton allocations. Differently, despite a remarkable blue/yellow intensity ratio identical to that of DCzSPOTz-based analogs, PhCzSPOTz still provided its UTBL WOLEDs with efficiencies almost equal to those of the corresponding yellow diodes, reflecting the complementary behaviour of TBPe and TBRb in

exciton harvesting. It is rational that the discrepancy between PhCzSPOTz and DCzSPOTz-based UTBL WOLEDs originated from the different exciton allocations between UTBLs and yellow EMLs. Judging from the efficiency correlations between blue, yellow and UTBL diodes, both singlet and triplet excitons were synchronously transferred to TBPe in DCzSPOTz hosted UTBL WOLEDs, therefore aggravating triplet quenching. On the contrary, considering singlet allocation to TBPe did not reduce EL efficiencies, and TBPe was actually excluded from triplet-involved processes in PhCzSPOTz based UTBL diodes.

### 2.3. Gaussian simulation

On the basis of molecular packings in single crystals, we simulated excited-state diffusion in PO dimers, with natural transition orbital (NTO) analysis (Fig. 3). Compared to its monomer, the singlet “hole” and “particle” of the DCzSPOTz dimer were almost uniformly dispersed on two molecules (Fig. 3a). It is noted that the dimerization markedly enhances the localization of the “hole” and “particle”, respectively, on the Cz and Tz groups, reducing the “hole”-“particle” overlap. Therefore, in spite of the symmetric distribution-induced near-zero centroid distance between the “hole” and “particle”, the overlap integrals of frontier molecular orbital (FMO) wave functions ( $\Psi_{\text{H}}|\Psi_{\text{L}}$ ) and electron cloud densities ( $\Psi_{\text{H}}^2|\Psi_{\text{L}}^2$ ) for the DCzSPOTz dimer are still smaller than those of its monomer (Fig. 3b). The situation of the  $T_1$  state for the DCzSPOTz dimer is the same, which shows the marked bimolecular dispersal uniformity and FMO separation. As a consequence, stronger  $\pi$ - $\pi$  interactions between adjacent Cz groups enhance intermolecular CT of the DCzSPOTz dimer, leading to a  $\Delta E_{\text{ST}}$  reduction to 0.27 eV and both singlet and triplet diffusion, which undoubtedly facilitate triplet diffusion in the DCzSPOTz matrix and to the UTBL interface during the EL process. At the other extreme is DPhSPOTz, whose dimer has the unchanged  $S_1$  and  $T_1$  energy levels and diphenyltriazine-localized excited states identical to those of the monomer.

Differently, the singlet “hole” and “particle” of the PhCzSPOTz dimer are still mainly localized on one molecule, but the partial “hole” is dispersed on the other molecule, resulting in increased singlet  $d_{\text{H-L}}$  and decreased singlet ( $\Psi_{\text{H}}|\Psi_{\text{L}}$ ) and ( $\Psi_{\text{H}}^2|\Psi_{\text{L}}^2$ ); meanwhile, triplet “hole” and “particle” distributions of the PhCzSPOTz dimer are identical to those of the monomer, namely thoroughly localized on a single molecule, in accord with the unchanged NTO parameters of the triplet states. Therefore, in addition to a slight  $\Delta E_{\text{ST}}$  reduction to 0.20 eV, weaker but effective intermolecular interaction in the PhCzSPOTz dimer induces sufficient singlet diffusion, but simultaneously averts undesired triplet diffusion. It is rational that the selectively controlled exciton diffusion in PhCzSPOTz based UTBL WOLEDs facilitated singlet exciton harvesting by FL emitters, and simultaneously suppressed diffusion-induced triplet quenching.

### 2.4. Optical properties

To figure out energy transfer processes, we investigate the photophysical properties of the non-doped and doped films (Fig. 4 and S20–S25†). In neat films, emissions of DCzSPOTz and PhCzSPOTz shift slightly to 472 and 484 nm (Fig. 4a and



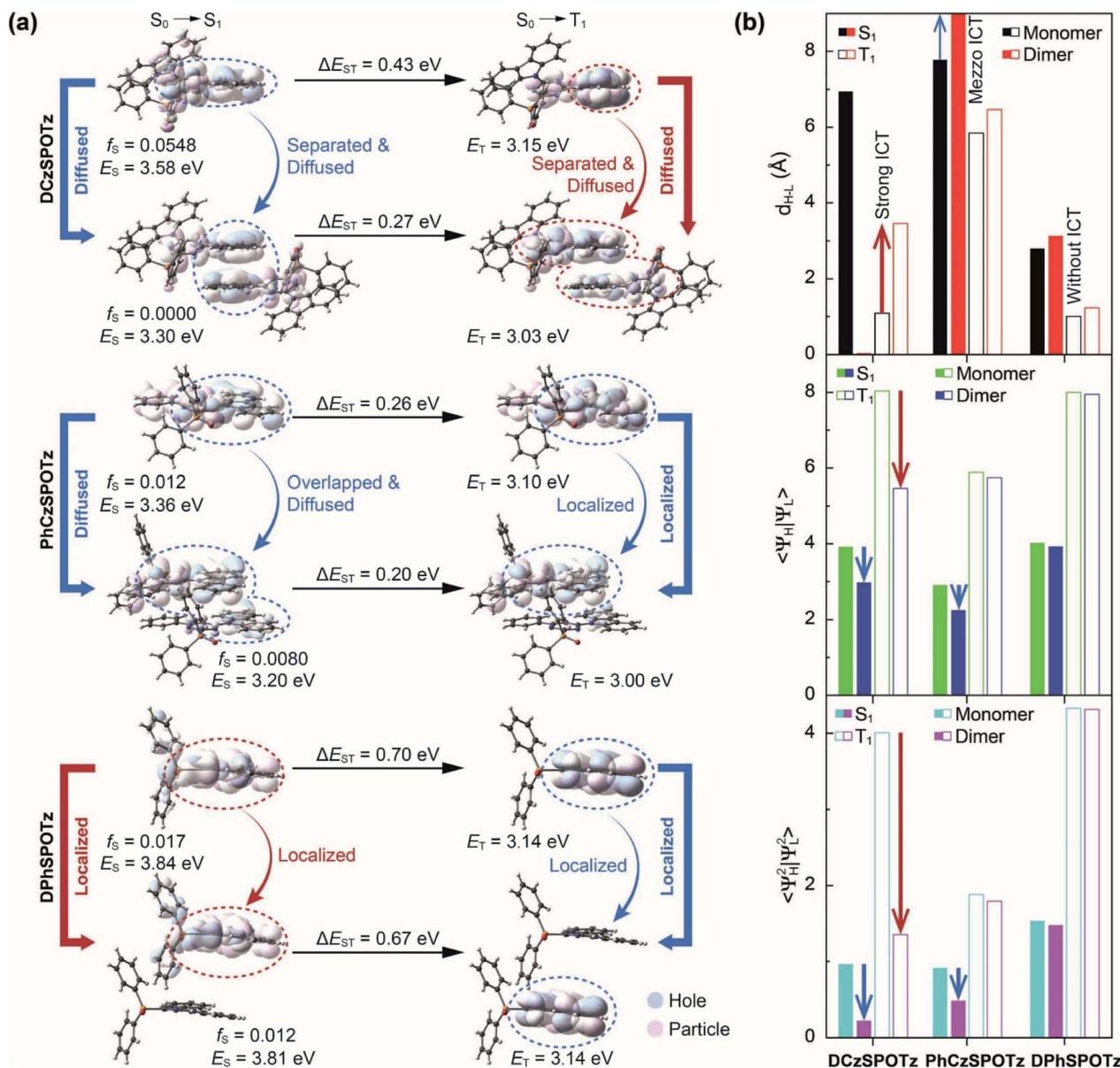


Fig. 3 Simulation results by time-dependent density functional theory. (a) Comparisons between "hole" (cyan) and "particle" (pink) contours, the  $S_1$  ( $E_S$ ) and  $T_1$  ( $E_T$ ) energy levels, singlet-triplet splitting energies ( $\Delta E_{ST}$ ) and singlet oscillator strengths ( $f_S$ ) of the monomers and dimers of DCzTzSPO, PhCzSPOTz and DPhTzSPO simulated with natural transition orbital analysis, respectively; (b) orbital parameter variations of the  $S_1$  and  $T_1$  states of the monomers and dimers of DCzTzSPO, PhCzSPOTz and DPhTzSPO.  $d_{H-L}$ ,  $\Psi_H|\Psi_L$  and  $\Psi_H^2|\Psi_L^2$  refer to the centroid distances, wavefunction overlap integral and electron-cloud overlap integral between the "holes" and "particles", respectively.

Table S1†). DPhSPOTz reveals an excimer-originated peak at  $\sim 490$  nm, which provides a channel for RISC. The PL quantum yield (PLQY,  $\eta_{PL}$ ) of the neat PhCzSPOTz film is 28%, slightly higher than 25% of DCzSPOTz and far exceeding 3.6% of DPhSPOTz (Table S3†). 1% TBPe doped films reveal pure blue emissions from the dopant, reflecting the complete energy transfer (Fig. 4a). The PL spectrum of the PhCzSPOTz:1% TBPe film is markedly broadened, due to intermolecular charge transfer interactions between PhCzSPOTz and TBPe; while, the DCzSPOTz:1% TBPe film reveals the narrowest PL spectrum, owing to the largest steric hindrance of DCzSPOTz. It is noted that  $\eta_{PL}$  of the DPhSPOTz:1% TBPe film of 36.2% is the highest.

The PhCzSPOTz:1% TBPe film roughly preserves the intrinsic  $\eta_{PL}$  of the host, but  $\eta_{PL}$  of the DCzSPOTz:1% TBPe film is nearly halved. Obviously,  $\eta_{PL}$  values of these TBPe doped films are in reverse proportion to triplet diffusibilities of the PO matrices. Different to 3% TBRb doped DCzSPOTz and PhCzSPOTz films with pure yellow emissions, host-originated emission can be recognized at 400–500 nm for the DPhSPOTz:3% TBRb film, due to a too large host-dopant singlet energy gap of 1.3 eV. Nevertheless,  $\eta_{PL}$  values of 3% TBRb doped DCzSPOTz, PhCzSPOTz and DPhSPOTz films are dramatically increased to 90.9%, 99.0% and 26.3%, respectively, owing to the EG effect suppressed triplet quenching by TBRb.



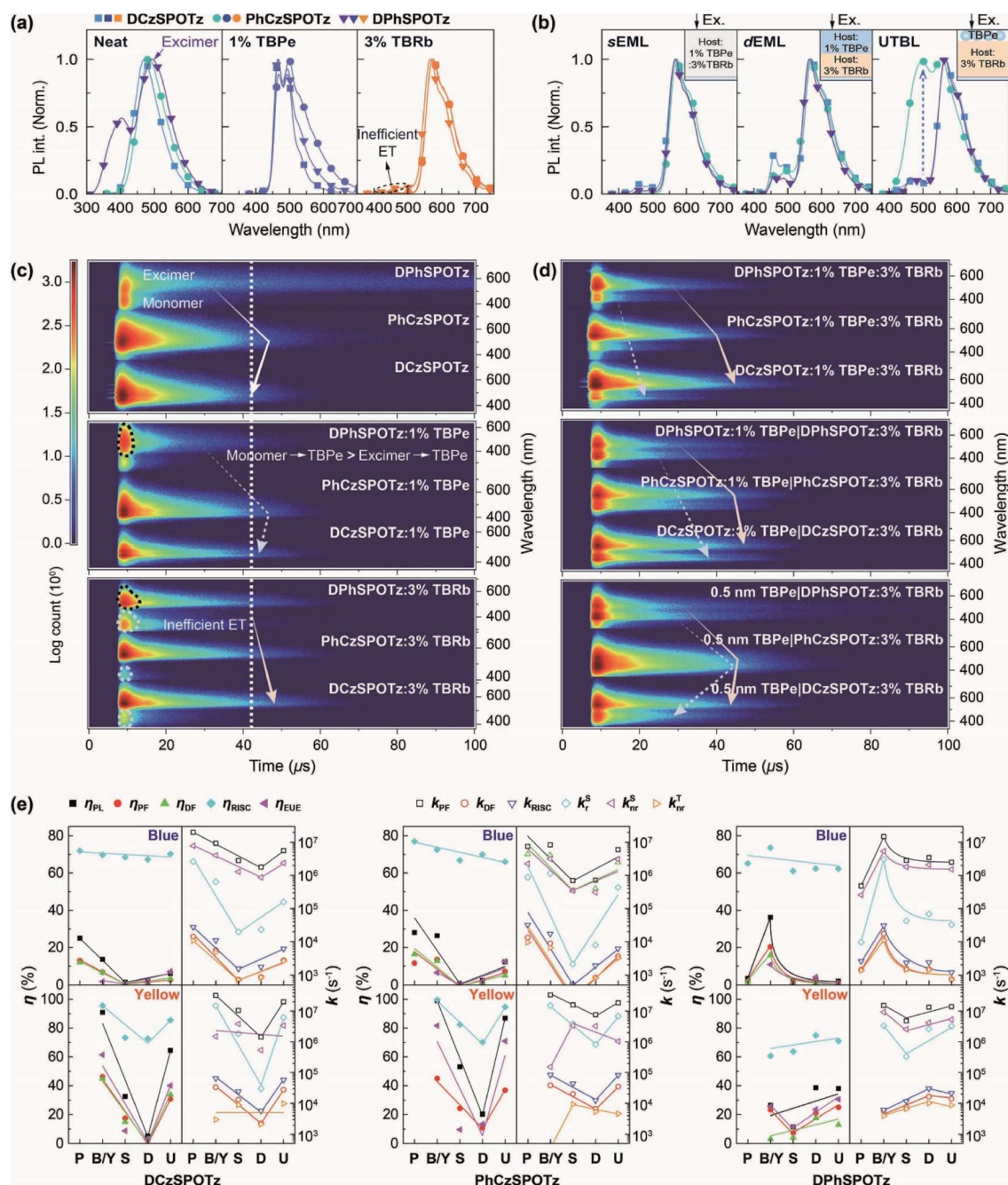


Fig. 4 Photophysical properties of the films. (a) Steady-state photoluminescence (PL) spectra of vacuum-evaporated neat, 1% TBPe and 3% TBRb doped DCzSPOTz, PhCzSPOTz, and DPhSPOTz films; (b) PL spectra of single-layer (host:1% TBPe:3% TBRb), dual-layer (host:1% TBPe|host:3% TBRb) and UTBL-type (TBPe (1 nm)|host:3% TBRb) films, corresponding to the sEML, dEML and UTBL-EML in the WOLEDs. Insets show the film structures; (c) transient emission contours of vacuum-evaporated neat, 1% TBPe and 3% TBRb doped DCzSPOTz, PhCzSPOTz, and DPhSPOTz films, in which the arrows respectively highlight the delayed fluorescence (DF) reduction and increase; (d) transient emission contours of vacuum-evaporated sEML, dEML and UTBL-type white-emitting films, in which the blue dashed and yellow solid arrows highlight the DF reduction and increases of TBPe and TBRb emissions, respectively; (e) photophysical parameters of pure films (P), blue or yellow films (B/Y), single-layer (S) and dual-layer (D) white-emitting films, and quasi-dual-layer white-emitting films with ultrathin blue layers (U).  $\eta$  and  $k$  refer to the quantum efficiency and rate constant. Subscripts of PL, PF, DF, RISC, r and nr correspond to photoluminescence, prompt fluorescence, delayed fluorescence, reverse intersystem crossing, radiation and non-radiation, respectively. Superscripts of S and T correspond to singlet and triplet, respectively.

Similar to the EL spectra (Fig. S10–S12<sup>†</sup>), yellow components are predominant in the PL spectra of sEML-type films (Fig. 4b). Compared to the corresponding blue/yellow films,  $\eta_{\text{PL}}$  values of

blue and yellow components of sEML-type films are halved, especially for their blue  $\eta_{\text{PL}}$  values <3% (Table S3<sup>†</sup>). dEML and UTBL-type films were excited from the sides of TBPe-

incorporated layers to avert direct exciton confinement by TBRb. It is shown that the blue intensities of DCzSPOTz and PhCzSPOTz hosted dEML films are stronger than those of DPhSPOTz based analogs, which is in accord with the corresponding EL spectra. Nevertheless, both blue and yellow  $\eta_{\text{PL}}$  values of the latter are the highest among dEML films, and also higher than the DPhSPOTz based sEML film, which in turn indicates that doubled dopant quenching occurred in DCzSPOTz and PhCzSPOTz based films with reduced  $\eta_{\text{PL}}$  values. For UTBL films, due to excitation at the sides of the TBPe layers, at least some of the excitons were directly formed in the TBPe layers. In addition, because of spatial separation, energy transfer from PO matrices to TBPe thin layers should be through singlet-based FRET channels. Since the absorption section of PhCzSPOTz is markedly larger than that of DCzSPOTz and DPhSPOTz (Fig. 1d), PhCzSPOTz can support more efficient FRET to the TBPe thin layer, rendering the significantly bigger blue emissions from PhCzSPOTz-based UTBL films. In contrast to the unchanged  $\eta_{\text{PL}}$  values of DPhSPOTz based analogs, the total  $\eta_{\text{PL}}$  value of the 1 nm TBPe|PhCzSPOTz:3% TBRb film reaches 99.2%, equal to that of the corresponding yellow film. Similarly, the DCzSPOTz hosted UTBL film also shows a recovered total  $\eta_{\text{PL}}$  value of 70.7%. Moreover, compared to their sEML and dEML type analogs, the UTBL structure endows DCzSPOTz and PhCzSPOTz based films with both the highest blue and yellow  $\eta_{\text{PL}}$  values, manifesting synergistic spatial and EG effects on quenching suppression.

Time-resolved transient emission spectra (TRES) show that compared to neat PO films and PO:3% TBRb films with similar delayed fluorescence (DF) characteristics, DF proportions of all PO:1% TBPe films are reduced, reflecting triplet quenching by TBPe (Fig. 4c). DF components in the spectra of DPhSPOTz based films demonstrate the effective RISC channel provided by the DPhSPOTz excimer. It is noted that PhCzSPOTz can support the most efficient energy transfer to TBRb. The intensity of host self-emission of PO:3% TBRb films is directly proportional to the  $S_1$  and  $T_1$  levels of PO molecules, which is in accordance with the EG rule. For sEML-type white-emitting films using DPhSPOTz, PhCzSPOTz and DCzSPOTz matrices, blue and yellow DF proportions gradually increase, which is consistent with the exciton diffusion abilities of the host matrices (Fig. 4d). The employment of the dEML structure hardly changes the yellow prompt fluorescence (PF) and DF proportions, but markedly enhances blue PF and DF proportions due to spatial separation-hindered blue-to-yellow energy transfer. Similarly, the UTBL structure also enhances blue proportions. It is significantly noted that opposite to DCzSPOTz, blue DF intensities of DPhSPOTz and PhCzSPOTz hosted UTBL films are even stronger than those of their dEML films, which means that the UTBL strategy can support sufficient exciton allocation to TBPe, and simultaneously facilitate host-TBPe quenching.

It is shown that compared to singly doped blue films, radiative blue efficiencies ( $\eta$ ) and transition rate constant ( $k$ ) values of sEML and dEML films are sharply reduced by at least one order of magnitude (Fig. 4e and Table S3†). As a typical example, the blue singlet radiative rate constant ( $k_{\text{r}}^{\text{S}}$ ) of PhCzSPOTz:1% TBPe:3% TBRb is nearly zero ( $<10^3 \text{ s}^{-1}$ ), in comparison to  $1.13$

$\times 10^6 \text{ s}^{-1}$  for PhCzSPOTz:1% TBPe. Furthermore, it is noteworthy that the yellow triplet non-radiative rate constants ( $k_{\text{nr}}^{\text{T}}$ ) of PhCzSPOTz and DCzSPOTz hosted sEMLs are about twice of those of their dEMLs, manifesting TBPe with the intermediate  $T_1$  level induced triplet leakage to TBRb. Nevertheless, contrary to the situation of DPhSPOTz hosted films, yellow  $k_{\text{RISC}}$  and  $k_{\text{r}}^{\text{S}}$  values of PhCzSPOTz and DCzSPOTz based dEMLs are even lower than those of their sEMLs. It is shown that yellow  $k_{\text{RISC}}$  and  $k_{\text{r}}^{\text{S}}$  values of these dEMLs are in reverse proportion to exciton diffusibilities of their hosts, namely  $\text{DPhSPOTz} > \text{PhCzSPOTz} > \text{DCzSPOTz}$ . In this sense, despite alleviating blue emission quenching, interlayer singlet and triplet diffusion also decrease yellow TADF properties of PhCzSPOTz and DCzSPOTz based films, rendering a decrease of their whole white efficiencies. The UTBL strategy simultaneously and effectively solves the issue of interlayer exciton diffusion and triplet leakage to TBPe. As a consequence, for DCzSPOTz and PhCzSPOTz based UTBL films, besides 2.5 and 5 fold increased blue and 12 and 4 fold increased yellow  $\eta_{\text{PL}}$  values, respectively, their blue  $k_{\text{RISC}}$  and  $k_{\text{r}}^{\text{S}}$  values are largely increased by 4 and 8 fold, and 3.5 and 43 fold, respectively; meanwhile, their yellow  $k_{\text{RISC}}$  and  $k_{\text{r}}^{\text{S}}$  are also markedly improved by 200 and 10 fold, and 6 and 8 fold, respectively. Yellow  $\eta_{\text{RISC}}$  values of DCzSPOTz and PhCzSPOTz based UTBL films also recovered to 86% and 95%, close to the initial values (96% and 100%) of their yellow films.

## 2.5. Exciton kinetic analysis

It is noted that the electrical performance of the hosts is in accord with their carbazole number and triazine exposure degree (Fig. S26 and S27†). The hole transporting abilities of DCzSPOTz, PhCzSPOTz and DPhSPOTz decrease, but their electron transporting abilities increase. Compared to unipolar DPhSPOTz, ambipolar structures of DCzSPOTz and PhCzSPOTz induce the balance of hole and electron transportation in their UTBL devices (Fig. S27a†). Nevertheless, efficiencies of WOLEDs were not directly related to the electrical properties of the hosts, indicating the predominance of the exciton allocation process for exciton harvesting (Table S2†). Furthermore, IV characteristics of sEML, dEML and UTBL type WOLEDs based on PhCzSPOTz were comparable, indicating the similar recombination zones in these devices.

Exciton kinetics of WOLEDs are investigated with steady-state and time-resolved EL spectra (Fig. 5 and S28–S32†). Direct carrier capture and recombination on TBRb enhance yellow predominance of EL spectra for sEML type WOLEDs (Fig. 5a). On the contrary, the steady-state EL spectra of dEML and UTBL type WOLEDs are similar to the corresponding PL spectra. In DCzSPOTz based dEML devices, excitons are independently formed in blue and yellow EMLs nearly at the same time, due to the most efficient exciton diffusion. Moreover, blue-to-yellow energy transfer is limited. In comparison, excitons are mainly formed in yellow EMLs of PhCzSPOTz and DPhSPOTz based dEML devices, but in contrast to the latter with yellow-predominant emission, PhCzSPOTz still supports exciton diffusion from yellow to blue EMLs. It is noted that different to





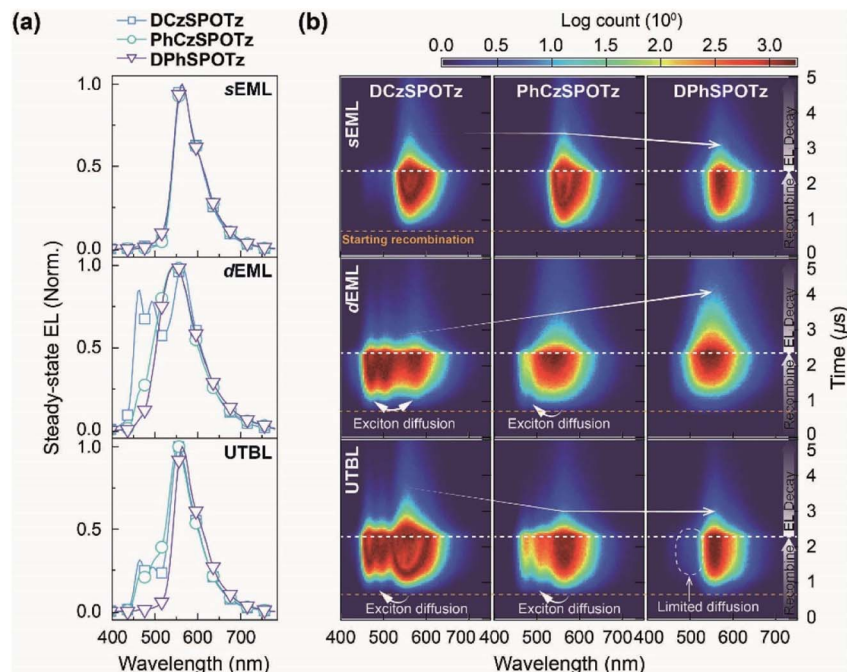


Fig. 5 EL kinetic analysis of HF WOLEDs. Dependence of (a) steady-state (left) and (b) transient (right) EL emission processes in sEML, dEML and UTBL type WOLEDs on hosts and EML structures. ET refers to energy transfer, respectively. Recombination start times are highlighted with yellow dashed lines.

sEML type WOLEDs with the consistent PL and EL DF variations, EL DF lifetimes of dEML WOLEDs are gradually increased, which is consistent to the order of their  $\eta_{\text{EQE}}$ , but opposite to the variation tendency of PL DF lifetimes of DCzSPOTz, PhCzSPOTz and DPhSPOTz, which manifests more significant contributions of exciton diffusion to EL quenching of TADF sensitized WOLEDs.

For all UTBL type WOLEDs, excitons are first formed in yellow EMLs with nearly the same recombination start times, which means the influence of the carrier transport difference on the recombination time can be negligible (Fig. 5b). Due to the limited exciton diffusion, DPhSPOTz based UTBL WOLEDs show a nearly pure yellow emission, but DCzSPOTz and PhCzSPOTz support effective exciton diffusion to the TBPe layer, rendering a significant blue component. Nonetheless, more direct exciton allocation to TBRb reduced blue components from TBPe, rendering the similar EL spectra of the latter, which were different to their PL spectra. It is noteworthy that despite the superiority of DCzSPOTz in exciton diffusion, the blue intensity of its UTBL WOLEDs is similar to that of PhCzSPOTz based analogs, indicating that more triplet excitons diffused to TBPe in the former. Simultaneously, exciton diffusion elongates the EL DF lifetime, and therefore worsens exciton quenching in DCzSPOTz based WOLEDs. With the appropriate exciton diffusibility, PhCzSPOTz not only endows its UTBL devices with desired white emissions, but also averts exciton-diffusion induced quenching. In this sense, the PhCzSPOTz matrix supports the “ideal” balance between spatial and EG effects of the UTBL strategy for simultaneously

optimizing blue and yellow components, therefore resulting in the state-of-the-art performance of HF WOLEDs.

### 3. Experimental section

#### 3.1. General procedure of the phosphorylation reaction

In  $\text{N}_2$ , diphenylphosphine (2.6 mL, 15 mmol) and 10 mmol of monochlorides (1, 3 and 4) were added into 20 mL of DMF. The mixtures were stirred for 24 h at 110 °C. The reactions were then cooled to room temperature and quenched by 50 mL of water. The mixtures were extracted with DCM ( $3 \times 20$  mL). 30%  $\text{H}_2\text{O}_2$  (5.7 mL, 50 mmol) was added dropwise into the combined DCM solutions at 0 °C. After stirring for 3 h, the reactions were quenched by the addition of 30 mL of sodium hydrogen sulfite. The mixtures were then extracted again with DCM ( $3 \times 10$  mL). The organic layers were combined, and dried with anhydrous  $\text{Na}_2\text{SO}_4$ . The solvent was removed by rotary evaporation, and the residues were purified by column chromatography. DCzSPOTz, DPhSPOTz and PhCzSPOTz as white powders were obtained with respective yields of 63%, 75% and 69%.

#### 3.2. (4,6-Di(9H-carbazol-9-yl)-1,3,5-triazin-2-yl) diphenylphosphine oxide (DCzSPOTz)

$^1\text{H}$  NMR (TMS,  $\text{CDCl}_3$ , 400 MHz):  $\delta$  = 8.628 (d,  $J$  = 8.0 Hz, 4H); 8.082 (dd,  $J_1$  = 12 Hz,  $J_2$  = 7.2 Hz, 4H); 8.008 (d,  $J$  = 8.0 Hz, 4H); 7.700 (t,  $J$  = 7.4 Hz, 2H); 7.602 (td,  $J_1$  = 7.6 Hz,  $J_2$  = 2.8 Hz, 4H); 7.390 (t,  $J$  = 7.2 Hz, 4H); 7.338 ppm (t,  $J$  = 7.2 Hz, 4H); LDI-MS:  $m/z$  (%): 611 (100) [ $\text{M}^+$ ]; elemental analysis (%) for  $\text{C}_{39}\text{H}_{36}\text{N}_5\text{OP}$ : C 76.59, H 4.28, and N 11.45; found: C 76.58, H 4.29, and N 11.47. CCDC Number: 2099961.

### 3.3. (4-(9*H*-Carbazol-9-yl)-6-phenyl-1,3,5-triazin-2-yl)diphenylphosphine oxide (PhCzSPOTz)

<sup>1</sup>H NMR (TMS, CDCl<sub>3</sub>, 400 MHz):  $\delta$  = 8.620 (d,  $J$  = 7.2 Hz, 4H); 8.036 (dd,  $J_1$  = 12 Hz,  $J_2$  = 7.2 Hz, 4H); 7.984 (d,  $J$  = 5.2 Hz, 2H); 7.650 (m, 3H); 7.573 (m, 6H); 7.378 ppm (m, 4H); LDI-MS:  $m/z$  (%): 522 (100) [M<sup>+</sup>]; elemental analysis (%) for C<sub>33</sub>H<sub>23</sub>N<sub>4</sub>OP: C 75.85, H 4.44, and N 10.72; found: C 75.85, H 4.44, and N 10.72. CCDC Number: 1838786.

### 3.4. (4,6-Diphenyl-1,3,5-triazin-2-yl)diphenylphosphine oxide (DPhSPOTz)

<sup>1</sup>H NMR (TMS, CDCl<sub>3</sub>, 400 MHz):  $\delta$  = 8.620 (d,  $J$  = 8.8 Hz, 4H); 8.030 (dd,  $J_1$  = 12 Hz,  $J_2$  = 8.4 Hz, 4H); 7.606 (t,  $J$  = 7.2 Hz, 4H); 7.523 ppm (t,  $J$  = 7.6 Hz, 8H); LDI-MS:  $m/z$  (%): 433 (100) [M<sup>+</sup>]; elemental analysis (%) for C<sub>27</sub>H<sub>20</sub>N<sub>3</sub>OP: C 74.82, H 4.65, and N 9.69; found: C 74.83, H 4.64, and N 9.71. CCDC Number: 1838785.

## 4. Conclusions

In summary, we demonstrate the state-of-the-art HF WOLEDs based on a non-doped ultrathin blue-emitting layer (0.1 nm) and a TADF sensitized yellow-emitting layer with a high doping concentration (3%). A record-high  $\eta_{\text{PE}}$  of  $\sim 80 \text{ lm W}^{-1}$  and an impressive  $\eta_{\text{EQE}}$  over 20% were achieved. The effectiveness of such an "UTBL" strategy relies on the combination of spatial and EG effects, in which triplet leakages in blue and yellow EMLs are averted by incorporating a host-free structure and a high-energy-gap TADF sensitizer matrix, respectively. To further optimize exciton diffusion in and between EMLs, asymmetric TADF sensitizer PhCzSPOTz is constructed, which can selectively support singlet exciton diffusion to TBPe and TBRb for improving their radiative efficiencies, but simultaneously suppress triplet-diffusion induced quenching. These results suggest that the synergetic material and device structure engineering provides a feasible way to overcome the challenge of HF WOLEDs in rational exciton allocation, which opens up another possibility of developing low-cost high-efficiency OLED lighting.

## Data availability

All data related to this paper can be requested from the authors.

## Author contributions

H. X. conceived the projects. C. D., Y. X., Z. W. and J. Z. performed the experiments. C. D., Y. X., C. H. and H. X. analyzed the data and wrote the paper. All authors commented on the manuscript.

## Conflicts of interest

There are no conflicts to declare.

## Acknowledgements

This study was supported by the National Natural Science Foundation of China (92061205, 51873056, U1801258, 61905070 and 22005088) and the Young Innovative Team Supporting Projects of Heilongjiang Province.

## Notes and references

- 1 K. T. Kamtekar, A. P. Monkman and M. R. Bryce, *Adv. Mater.*, 2010, **22**, 572–584.
- 2 G. M. Farinola and R. Ragni, *Chem. Soc. Rev.*, 2011, **40**, 3467–3482.
- 3 H. Wu, L. Ying, W. Yang and Y. Cao, *Chem. Soc. Rev.*, 2009, **38**, 3391–3400.
- 4 J. Kido, M. Kimura and K. Nagai, *Science*, 1995, **267**, 1332–1334.
- 5 S. Reineke, F. Lindner, G. Schwartz, N. Seidler, K. Walzer, B. Lussem and K. Leo, *Nature*, 2009, **459**, 234–238.
- 6 H. Uoyama, K. Goushi, K. Shizu, H. Nomura and C. Adachi, *Nature*, 2012, **492**, 234–238.
- 7 T. J. Penfold, F. B. Dias and A. P. Monkman, *Chem. Commun.*, 2018, **54**, 3926–3935.
- 8 Z. Yang, Z. Mao, Z. Xie, Y. Zhang, S. Liu, J. Zhao, J. Xu, Z. Chi and M. P. Aldred, *Chem. Soc. Rev.*, 2017, **46**, 915–1016.
- 9 J. Huang, H. Nie, J. Zeng, Z. Zhuang, S. Gan, Y. Cai, J. Guo, S.-J. Su, Z. Zhao and B. Z. Tang, *Angew. Chem., Int. Ed.*, 2017, **56**, 12971–12976.
- 10 Z. Li, D. Yang, C. Han, B. Zhao, H. Wang, Y. Man, P. Ma, P. Chang, D. Ma and H. Xu, *Angew. Chem., Int. Ed.*, 2021, **60**, 14846–14851.
- 11 B. Zhao, H. Wang, C. Han, P. Ma, Z. Li, P. Chang and H. Xu, *Angew. Chem., Int. Ed.*, 2020, **59**, 19042–19047.
- 12 S. Y. Lee, T. Yasuda, Y. S. Yang, Q. Zhang and C. Adachi, *Angew. Chem., Int. Ed.*, 2014, **53**, 6402–6406.
- 13 Y. Li, X.-L. Li, D. Chen, X. Cai, G. Xie, Z. He, Y.-C. Wu, A. Lien, Y. Cao and S.-J. Su, *Adv. Funct. Mater.*, 2016, **26**, 6904–6912.
- 14 Y. Chen, S. Li, T. Hu, X. Wei, Z. Li, Y. Liu, J. Liu, R. Wang, Y. Yi, C. Zhao, Y. Wang and P. Wang, *J. Mater. Chem. C*, 2018, **6**, 2951–2956.
- 15 Y. Liu, X. Wei, Z. Li, J. Liu, R. Wang, X. Hu, P. Wang, T. Qi and Y. Wang, *Adv. Opt. Mater.*, 2018, **6**, 1800978.
- 16 B. Zhao, H. Zhang, Y. Miao, Z. Wang, L. Gao, H. Wang, Y. Hao and W. Li, *J. Mater. Chem. C*, 2018, **6**, 304–311.
- 17 J. Zhao, X. Chen, Z. Yang, Z. Chi, Z. Yang, Y. Zhang, J. Xu, Z. Chi and M. P. Aldred, *J. Mater. Chem. C*, 2018, **6**, 3226–3232.
- 18 C. Li, Y. Xu, Y. Liu, Z. Ren, Y. Ma and S. Yan, *Nano Energy*, 2019, **65**, 104057.
- 19 W. Li, B. Li, X. Cai, L. Gan, Z. Xu, W. Li, K. Liu, D. Chen and S.-J. Su, *Angew. Chem., Int. Ed.*, 2019, **58**, 11301–11305.
- 20 R. Wang, Y. Liu, T. Hu, X. Wei, J. Liu, Z. Li, X. Hu, Y. Yi, P. Wang and Y. Wang, *Org. Electron.*, 2019, **71**, 24–30.
- 21 F.-M. Xie, S.-J. Zou, Y. Li, L.-Y. Lu, R. Yang, X.-Y. Zeng, G.-H. Zhang, J. Chen and J.-X. Tang, *ACS Appl. Mater. Interfaces*, 2020, **12**, 16736–16742.



- 22 J. Hu, Q. Li, X. Wang, S. Shao, L. Wang, X. Jing and F. Wang, *Angew. Chem., Int. Ed.*, 2019, **58**, 8405–8409.
- 23 X.-K. Liu, Z. Chen, J. Qing, W.-J. Zhang, B. Wu, H. L. Tam, F. Zhu, X.-H. Zhang and C.-S. Lee, *Adv. Mater.*, 2015, **27**, 7079–7085.
- 24 D. Zhang, L. Duan, Y. Zhang, M. Cai, D. Zhang and Y. Qiu, *Light: Sci. Appl.*, 2015, **4**, e232.
- 25 Z. Wu, J. Luo, N. Sun, L. Zhu, H. Sun, L. Yu, D. Yang, X. Qiao, J. Chen, C. Yang and D. Ma, *Adv. Funct. Mater.*, 2016, **26**, 3306–3313.
- 26 P. Wei, D. Zhang, M. Cai, X. Song, Z. Wang and L. Duan, *Org. Electron.*, 2017, **49**, 242–248.
- 27 C. Wu, B. Wang, Y. Wang, J. Hu, J. Jiang, D. Ma and Q. Wang, *J. Mater. Chem. C*, 2019, **7**, 558–566.
- 28 J. Liang, C. Li, X. Zhuang, K. Ye, Y. Liu and Y. Wang, *Adv. Funct. Mater.*, 2018, **28**, 1707002.
- 29 Z. Wu, Y. Liu, L. Yu, C. Zhao, D. Yang, X. Qiao, J. Chen, C. Yang, H. Kleemann, K. Leo and D. Ma, *Nat. Commun.*, 2019, **10**, 2380.
- 30 C. Huang, Y. Zhang, J. Zhou, S. Sun, W. Luo, W. He, J. Wang, X. Shi and M.-K. Fung, *Adv. Opt. Mater.*, 2020, **8**, 2000727.
- 31 J. Zeng, J. Guo, H. Liu, Z. Zhao and B. Z. Tang, *Adv. Funct. Mater.*, 2020, **30**, 2000019.
- 32 C. Zhang, Y. Lu, Z. Liu, Y. Zhang, X. Wang, D. Zhang and L. Duan, *Adv. Mater.*, 2020, **32**, 2004040.
- 33 X.-L. Chen, J.-H. Jia, R. Yu, J.-Z. Liao, M.-X. Yang and C.-Z. Lu, *Angew. Chem., Int. Ed.*, 2017, **56**, 15006–15009.
- 34 L.-S. Cui, H. Nomura, Y. Geng, J. U. Kim, H. Nakanotani and C. Adachi, *Angew. Chem., Int. Ed.*, 2017, **56**, 1571–1575.
- 35 Y. Xu, C. Li, Z. Li, Q. Wang, X. Cai, J. Wei and Y. Wang, *Angew. Chem., Int. Ed.*, 2020, **59**, 17442–17446.
- 36 J. Sun, J. Zhang, Q. Liang, Y. Wei, C. Duan, C. Han and H. Xu, *Adv. Funct. Mater.*, 2020, **30**, 1908568.
- 37 D. Ding, Z. Wang, C. Li, J. Zhang, C. Duan, Y. Wei and H. Xu, *Adv. Mater.*, 2020, **32**, 1906950.
- 38 J. Zhang, Y. Wei and H. Xu, *Nano Energy*, 2021, **83**, 105746.
- 39 J. Zhang, C. Han, F. Du, C. Duan, Y. Wei and H. Xu, *Adv. Funct. Mater.*, 2020, **30**, 2005165.
- 40 T. Higuchi, H. Nakanotani and C. Adachi, *Adv. Mater.*, 2015, **27**, 2019–2023.
- 41 C. Han, R. Du, H. Xu, S. Han, P. Ma, J. Bian, C. Duan, Y. Wei, M. Sun, X. Liu and W. Huang, *Nat. Commun.*, 2021, **12**, 3640.
- 42 Y. Li, Z. Li, J. Zhang, C. Han, C. Duan and H. Xu, *Adv. Funct. Mater.*, 2021, **31**, 2011169.
- 43 H. Nakanotani, T. Higuchi, T. Furukawa, K. Masui, K. Morimoto, M. Numata, H. Tanaka, Y. Sagara, T. Yasuda and C. Adachi, *Nat. Commun.*, 2014, **5**, 4016.
- 44 D. Zhang, L. Duan, C. Li, Y. Li, H. Li, D. Zhang and Y. Qiu, *Adv. Mater.*, 2014, **26**, 5050–5055.
- 45 D. Zhang, X. Song, A. J. Gillett, B. H. Drummond, S. T. E. Jones, G. Li, H. He, M. Cai, D. Credgington and L. Duan, *Adv. Mater.*, 2020, **31**, 1908355.
- 46 D. Zhang, X. Song, M. Cai, H. Kaji and L. Duan, *Adv. Mater.*, 2018, **30**, 1705406.
- 47 D. Zhang, X. Song, M. Cai and L. Duan, *Adv. Mater.*, 2018, **30**, 1705250.
- 48 P. Wei, D. Zhang and L. Duan, *Adv. Funct. Mater.*, 2019, **29**, 1907083.
- 49 W. Song, I. Lee and J. Y. Lee, *Adv. Mater.*, 2015, **27**, 4358–4363.
- 50 Z. Wang, X.-L. Li, Z. Ma, X. Cai, C. Cai and S.-J. Su, *Adv. Funct. Mater.*, 2018, **28**, 201706922.
- 51 X. Tang, Y. Li, Y.-K. Qu, C.-C. Peng, A. Khan, Z.-Q. Jiang and L.-S. Liao, *Adv. Funct. Mater.*, 2020, **30**, 1910633.
- 52 L.-S. Cui, A. J. Gillett, S.-F. Zhang, H. Ye, Y. Liu, X.-K. Chen, Z.-S. Lin, E. W. Evans, W. K. Myers, T. K. Ronson, H. Nakanotani, S. Reineke, J.-L. Bredas, C. Adachi and R. H. Friend, *Nat. Photon.*, 2020, **14**, 636–642.
- 53 J.-i. Nishide, H. Nakanotani, Y. Hiraga and C. Adachi, *Appl. Phys. Lett.*, 2014, **104**, 233304.
- 54 J. Li, D. Ding, Y. Tao, Y. Wei, R. Chen, L. Xie, W. Huang and H. Xu, *Adv. Mater.*, 2016, **28**, 3122–3130.

